GENERAL CHARACTERISTICS OF HADRON

PRODUCTION AT SPEAR[*]

V. Lüth

Stanford Linear Accelerator Center
Stanford University, Stanford, California 94305

I.   INTRODUCTION

The very first and preliminary data on the production of hadrons by e^+e^- annihilation were presented at the Kiev Conference five years ago[1] causing great excitement. These first results from ADONE at Frascati were confirmed and the hadronic nature of the final states was proven in the years following. In Figure 1 the most recent update of the measurements at ADONE[2-5] are plotted along with other low energy data from Orsay[6] and Novosibirsk.[7] The quantity R, the ratio of the total hadron production to muon pair production is evaluated as a function of the c.m. energy $E_{c.m.}$ In spite of large errors and inconsistencies between various measurements, they clearly show that hadron production is substantial, i.e., it is comparable or greater than μ-pair production.
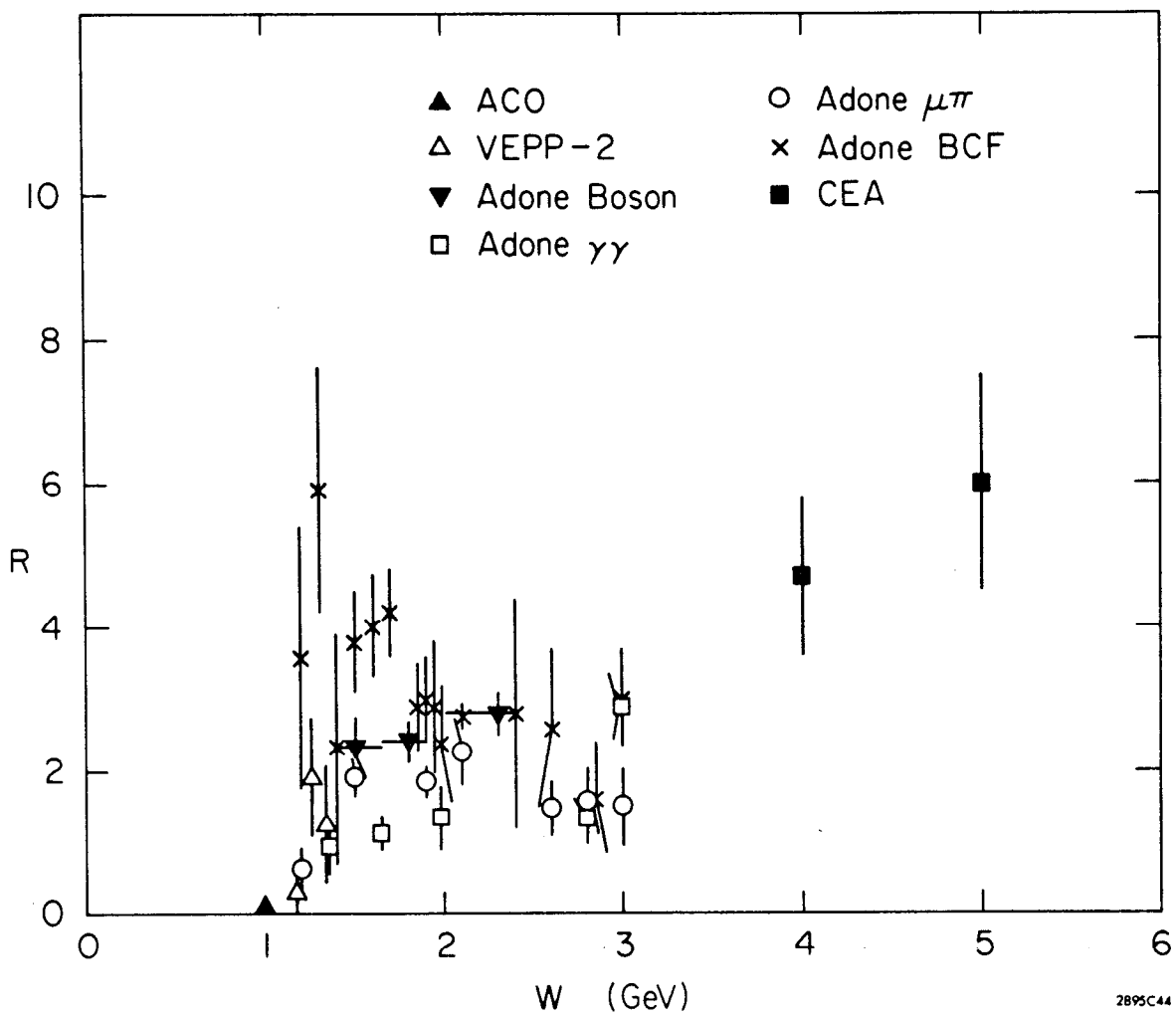
Fig. 1 Results on multihadron production by e^+e^- annihilation as a function of c.m. energy $E_{c.m.}$. Data from Frascati (ADONE),[2-5] Orsay (ACO),[6] Novosibirsk,[7] and Cambridge (CEA).[8]

By far the most serious problems these pioneering experiments at Frascati had to face came from the small solid angle of the detectors. They typically covered no more than 20% of 4π and were placed at interaction regions nearly as long as the detectors. With two charged particles required for triggering this lead to a total acceptance of 10% or less, introducing large systematic uncertainties.

The second generation results from the non-magnetic detector BOLD at CEA,[8] a device with much larger solid angle, was at first met with considerable skepticism. Low beam intensities limited these measurements to two energies, $E_{c.m.}$ = 4 GeV and $E_{c.m.}$ = 5 GeV. The results, indicating a significantly higher value of R have been confirmed by more recent data from SPEAR[9] and DORIS.[10,11]

In this report we shall discuss what we have learned about hadron production at SPEAR since the discovery of the two narrow resonances, ψ (3095)[12,13] and ψ (3684).[14] To a large extent, this will be an update of Roy Schwitter's presentation at the Photon-Lepton Symposium two years ago at Stanford.[15] In particular, we shall address ourselves to difficulties related to the model dependence of the detector efficiency and effects of the heavy lepton production. We shall include recent results on inclusive production of kaons, protons and Λ hyperons and their implications for charm particle production.

II. PARTON MODEL

Accepting the traditional concept that the electron does not directly couple to hadrons, the production of hadrons by e^+e^- annihilation proceeds dominantly via the exchange of a single, time-like photon between the lepton and the hadron system. Higher order photon exchange

processes generally produce particles at small angles to the beams. Since present detectors do not cover this angular range these processes are of limited importance to hadron production at present energies.

If we restrict ourselves to the one-photon photon exchange as the main process for hadron production by e^+e^- annihilation (Fig. 2a), we see that the annihilation itself is well understood in terms of a point-like lepton-hadron vertex, whereas all ignorance is hidden by the cross hatched region of the photon-hadron vertex. We know, however, that the hadron system must have the quantum numbers of the photon, i.e., $J^{PC} = 1^{--}$ and all additive quantum numbers are equal to zero. A comparison with the diagram for muon pair production in Fig. 2b illustrates that the quantity of more direct interest than the total hadronic cross section, σ_{had}, is R the ratio of hadron to muon pair production,

$$R = \frac{\sigma_{had}}{\sigma_{\mu\mu}} \text{ with } \sigma_{\mu\mu} = \frac{4\pi\alpha^2}{3 s} .$$

Here s is the square of the mass of the virtual photon and α the fine structure constant.

One of the most fundamental theoretical concepts for high energy particle physics is that of scaling. It says that σ_{had} should vary like $1/s$ for large s or stated differently, the ratio R is expected to approach a constant value; "large" generally means large compared to any mass or energy involved. The simplest argument to predict scaling is one of dimensional analysis. It says that at high energies the only unit of length is $s^{-1/2}$, thus a cross section must behave like s^{-1}.

A far more appealing picture that arrives at the same answer is the parton model.[16] Measurements of deep inelastic electron-nucleon
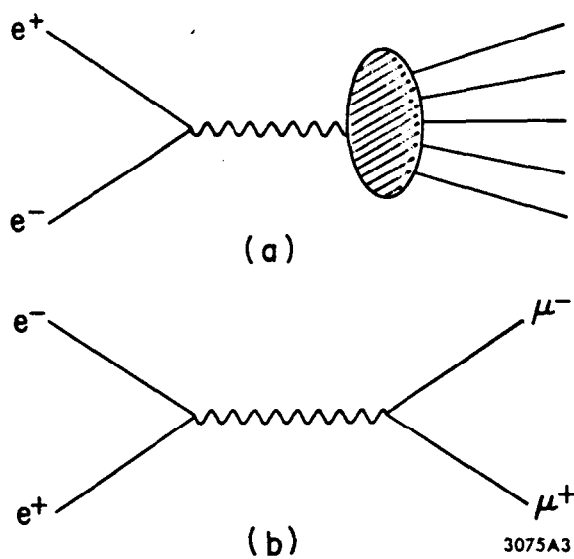
Fig. 2. Feynman diagrams for one-photon exchange
(a) $e^+e^- \rightarrow$ hadrons; (b) $e^+e^- \rightarrow \mu^+\mu^-$.

scattering led to the hypothesis that hadrons are built out of constituents, the partons, which have point-like coupling to the electromagnetic current. Thus, photon-hadron interactions are basically photon-parton interactions and consequently hadron production in e^+e^- annihilation proceeds via the formation of pairs of parton-antiparton. If partons have spin 1/2 then the cross section for producing the free $q_i\bar{q}_i$ pair is the same as for producing a $\mu^+\mu^-$ pair, except for the difference in electric charge Q_i,

$$(e^+e^- \to q_i\bar{q}_i) = Q_i^2 \, \sigma_{\mu\mu} \quad .$$

Assuming further that the $q_i\bar{q}_i$ pairs convert to hadrons with probability one, the hadronic cross section equals the sum of the individual parton pair cross section, and

$$R = \frac{\sigma_{had}}{\sigma_{\mu\mu}} = \sum_i Q_i^2 .$$

Given a fixed number of partons having specified charges Q_i, R is constant, and hadron production is said to exhibit scaling. Wherever a threshold for the production of higher mass constituents is reached, there should be an upward step in R proportional to Q_i^2 of the new parton. The value of R at any given energy provides information about the number and properties of the partons produced. Clearly, the existence of partons is purely hypothetical, but they help to explain a great deal of data.

If one associates partons with quarks of spin 1/2, available in 3 colors, then one obtains

$$R_{uds} = 3 \left((2/3)^2 + (1/3)^2 + (1/3)^2 \right) = 2;$$

and above charm threshold

$$R_{udsc} = 10/3.$$

Another consequence of this particular model of hadron production is the jet-like structure of the final states that arises due to limited transverse momenta of the hadrons relative to the parton direction of motion. The angular distribution of the jet-axis has been found to agree with the $1 + \cos^2\theta$ distribution expected for spin 1/2 parton-antiparton pair.[17]

Furthermore, the inclusive momentum spectra are expected to exhibit scaling at high energy. In complete analogy to deep inelastic ep scattering the most general form of the differential cross section can be written as a function of two structure functions W_o and W_1,

$$\frac{d^2\sigma}{dxd\Omega} = \frac{\alpha^2\beta}{4\pi} = [W_1(x,s) \ (1 + \cos^2\theta) + W_o(x,s) \ \sin^2\theta]$$

where

$$x = 2E_h/E_{c.m.} \ ; \ \beta = P_h/E_h$$

and P_h, E_h are respectively the momentum and energy of the hadron. If at sufficiently high energy W_o and W_1 become independent of x, dσ/dx will decrease like 1/s (Bjorken scaling) and the ratio R will be constant.

III. THE MAGNETIC DETECTOR AT SPEAR

The solenoidal magentic detector built and operated by the SLAC-LBL collaboration is shown in Fig. 3. It provides a nearly uniform field of 4 kG over a volume 3-m long and 3 m in diameter. A particle produced in the interaction region first traverses the 150 μm steel vacuum pipe,

MUON WIRE CHAMBERS
IRON (20 cm)
SHOWER COUNTERS (24)
COIL
TRIGGER COUNTERS (48)

CYLINDRICAL
WIRE CHAMBERS

TRIGGER
COUNTERS (4)

BEAM PIPE

PROPORTIONAL
CHAMBERS (2)

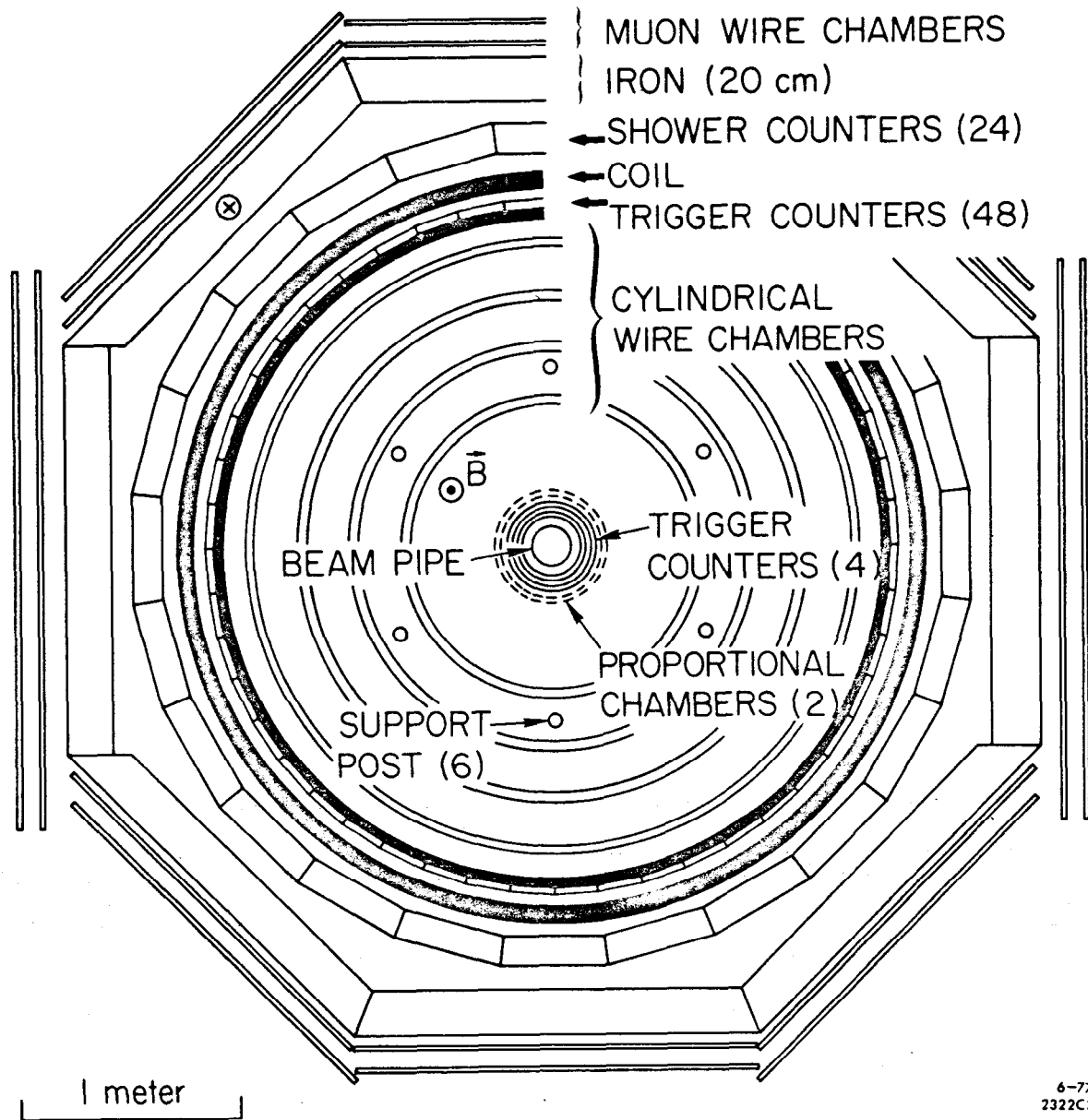SUPPORT
POST (6)

$\vec{B}$

1 meter

6-77
2322C3

Fig. 3. End view of the SLAC–LBL magnetic detector.

then a pair of cylindrical scintillation counters and two proportional

wire chambers that form an element of the trigger system. Continuing

outwards, the particle passes through 4 sets of magnetostrictive spark

chambers, a trigger hodoscope that provides time-of-flight measurements,

the one radiation length coil, and array of shower counters. Most

hadrons are absorbed in the 20 cm thick iron yoke and will not reach a

set of spark chambers outside that aids muon identification. The momen-

tum analysis (resolution $\Delta p/p = 0.015\ p$) and particle identification

of the detector extend over 65% of 4π; the azimuthal acceptance is com-

plete, and the subtended polar angle ranges for 50° to 130°. The

hardware trigger requires at least two charged particles each firing a

trigger counter and an associated shower counter in coincidence with the

beams. This requirement, which restricts the data sample to events with

at least two particles with momenta above 200 MeV/c, and the limited

solid angle of the apparatus are largely responsible for the uncertainties

in the cross section data.

The data analysis distinguishes two general categories of events,

lepton pairs

$$e^+e^- \to e^+e^-$$
$$e^+e^- \to \mu^+\mu^- \quad ,$$

and hadronic final states,

$$e^+e^- \to \text{hadrons}.$$

A hadronic event is required to have three or more tracks forming a

vertex within the luminous region of the machine. Two-prong events are

also included in the hadronic event sample provided the tracks are

acoplanar with the beams by at least 20° and have momenta exceeding 300 MeV/c.

IV. TOTAL CROSS SECTION

The major aim of the SLAC-LBL experiment was to obtain an accurate measurement of the total hadronic cross section σ_{had} over as wide a range in energy as the storage ring would allow. σ_{had} is given by

$$\sigma_{had} = \frac{\Sigma M_i}{\bar{\varepsilon} \int \mathscr{L} dt} , \qquad (1)$$

where M_i is the number of events observed with i charged tracks, $\bar{\varepsilon}$ the average efficiency of all events and $\int \mathscr{L} dt$ is the integrated luminosity as monitored by Bhabha scattering events in the same detector. The important factors limiting the precision of σ_{had} are (a) the statistical error of the event sample, (b) the level of background in the data, (c) the systematic error in the luminosity monitoring, and (d) the systematic errors in the evaluation of the detection efficiency. As we shall see, the last point is the most serious.

The raw number of detected events in the hadronic event class is first corrected for various sources of background. Beam-gas interactions are estimated from event rates just outside the interaction region. Beam-gas backgrounds amount typically to 6% of the total. Cosmic-ray background is suppressed to a negligibly low level by the TOF system. Contaminations due to electrodynamic final states arising from two-photon processes and radiative e^+e^- or $\mu^+\mu^-$ production are calculated to be of the order of a few percent. A correction is made to the two-prong events. Evidence for non-hadronic multibody final states originating from the production and decay of a pair of heavy leptons[18] will

be presented below. Such events should not be included in the hadronic cross section measurement. The average detection efficient $\bar{\varepsilon}$ is defined as the ratio of the number of events observed to the number of produced events, i.e.,

$$\bar{\varepsilon} = \sum_i M_i / \sum_j N_j , \tag{2}$$

where N_j is the number of events produced with j charged particles. Observed and produced multiplicities are related by

$$M_i = \sum_j \varepsilon_{ij} N_j , \tag{3}$$

where ε_{ij}' is the efficiency for detecting an event with i prongs, when it was produced with j charged particles. The matrix elements ε_{ij} are computed by a Monte Carlo simulation of the experiment. Known properties of the detector, such as solid angle, trigger biases, cuts in the data analysis, and a plausible model of the final states are necessary ingredients of such calculations. Given the coefficients ε_{ij}, Eq. (3) is inverted by a maximum likelihood fit to obtain the produced multiplicity distribution N_j, and thereby $\bar{\varepsilon}$.

Three different models of multihadron production have been used to check the sensitivity of $\bar{\varepsilon}$ to the choice of the model and to compare with the data. All pion final states are simulated by a two-jet model, in which the jet axis has a $1 + \cos^2\theta$ angular distribution and particles are emitted from each jet with transverse momenta limited by a matrix element of the form

$$|M|^2 = e^{-\sum p_{\perp i}^2 / 2b^2}$$

The total multiplicity and the charged multiplicity as well as the transverse momentum cut-off b and the orientation of the jet axis have been adjusted to agree with the data.[17] The production and decay of a pair of heavy leptons of mass 1.9 GeV is simulated in accordance with its predicted properties.[19] The third model reproduces the associated production of D and D^* mesons near threshold. All parameters like the masses, relative production rates and branching ratios have been chosen to agree with the data at 4.03 GeV.[20]

In the following we shall compare in some detail the observed and the Monte Carlo simulated distributions. The results are shown on an arbitrary scale with statistical errors only. In Figure 4 the momentum spectra are presented for selected c.m. energies, separately for 2-prongs and multiprongs. The normalization of the τ-pair Monte Carlo is absolute, the sum of all model calculations are normalized to the total number of events. At 4.03 GeV the pion model is normalized to fit the data for x < 0.6. Below charm threshold at 3 GeV the all pion jet model fits the data reasonably well, whereas the same model shows a strong disagreement with the data at 7.4 GeV, particularly for two-prong events. The difference can, to a large extent, be accounted for by the expected contribution from $\tau^+ \tau^-$ production. The remaining excess in the data at very small x can be explained by a contamination from two-photon processes that has not been subtracted in these plots. At 4.03 GeV the difference between the sum of pion and heavy lepton production is limited to x < 0.5 and can be well understood in terms of charm production near threshold. The discrepancy between the data and the jet model calculation can also be observed in the angular correlation of two prong events. The jet
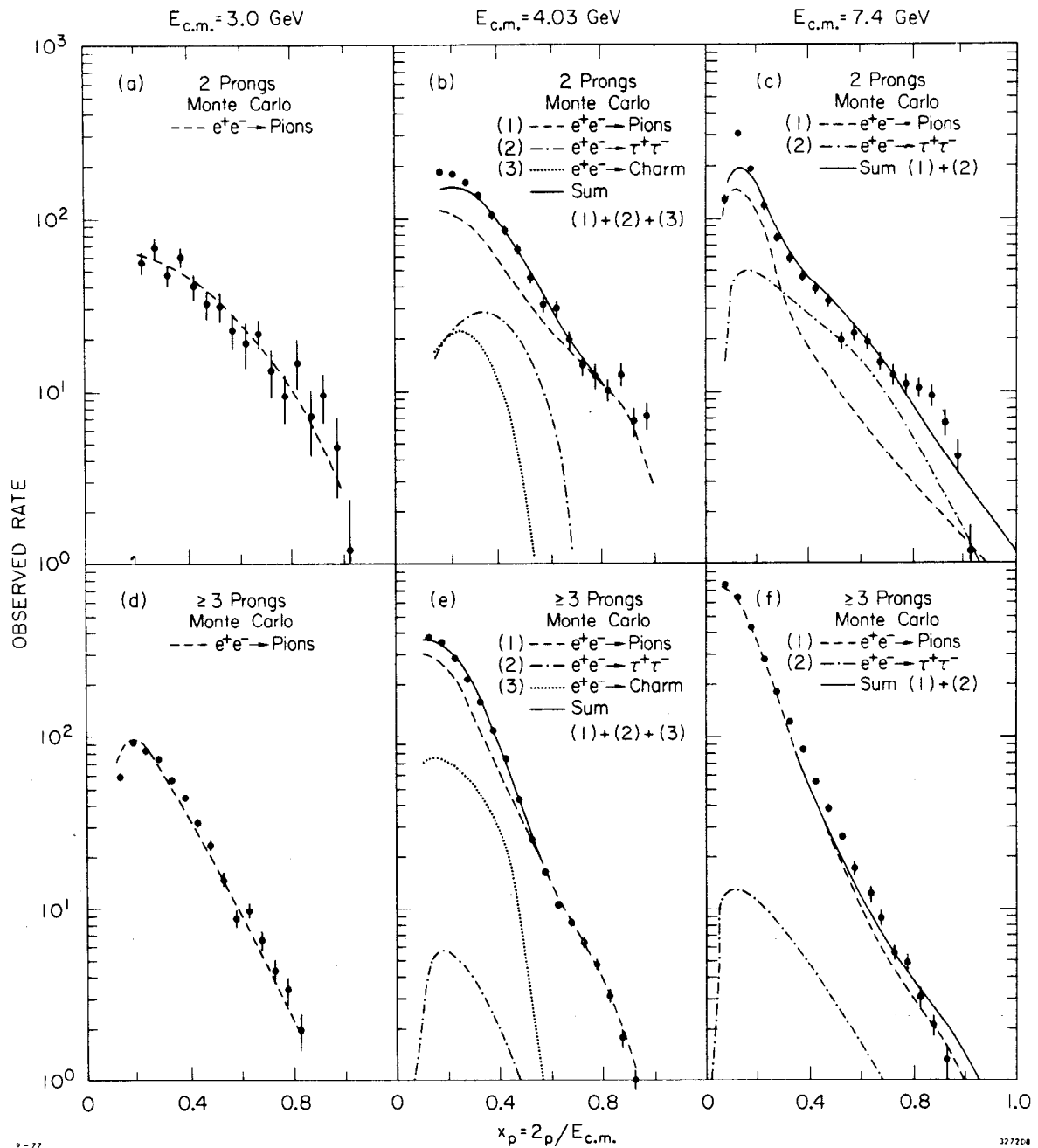
Fig. 4. Observed x distributions for charged particles at various energies. The data are compared to different Monte Carlo simulations. The errors are purely statistical.

model fails to reproduce the pronounced backward peak in the collinearity angle, while this enhancement is present in the heavy lepton simulation (Fig. 5) and can make up for this discrepancy. In conclusion, the high energy data indicate the presence of dynamics that cannot be described by a jet model for hadron production. The fact that the jet model simulation used here does not take into account the production of kaons, nucleons and other heavier particles may account for some differences between data and model, but it can hardly explain this large a discrepancy. If we accept the existence of such a heavy lepton, we should subtract this non-hadronic contribution from our data. In the following we shall take a double route by presenting the results with and without this subtraction. As a consequence we obtain two different multiplicity distributions and two different efficiency curves. If we include all events remaining in the hadronic category after subtraction of beam-gas and two-photon backgrounds, the average detection efficiency rises from roughly 35% at 3 GeV to 63% above 6 GeV (Figure 6a). The subtraction of events expected from $\tau^+\tau^-$ production predominantly affects the two-prong events and raises $\bar{\varepsilon}$ to more than 70% at high energy (Fig. 6b).

A complete, though preliminary, result on measurements of the hadronic cross section σ_{had} over the whole c.m. energy range of the SPEAR machine was first presented two years ago at Stanford.[15] Since then many aspects of the analysis have been improved and detailed studies of the detection efficiency have been performed. A present day update of the results is given in Fig. 7 in terms of R = $\sigma_{had}/\sigma_{\mu\mu}$. The difference to the earlier publication is fairly small, and the situation reminds me
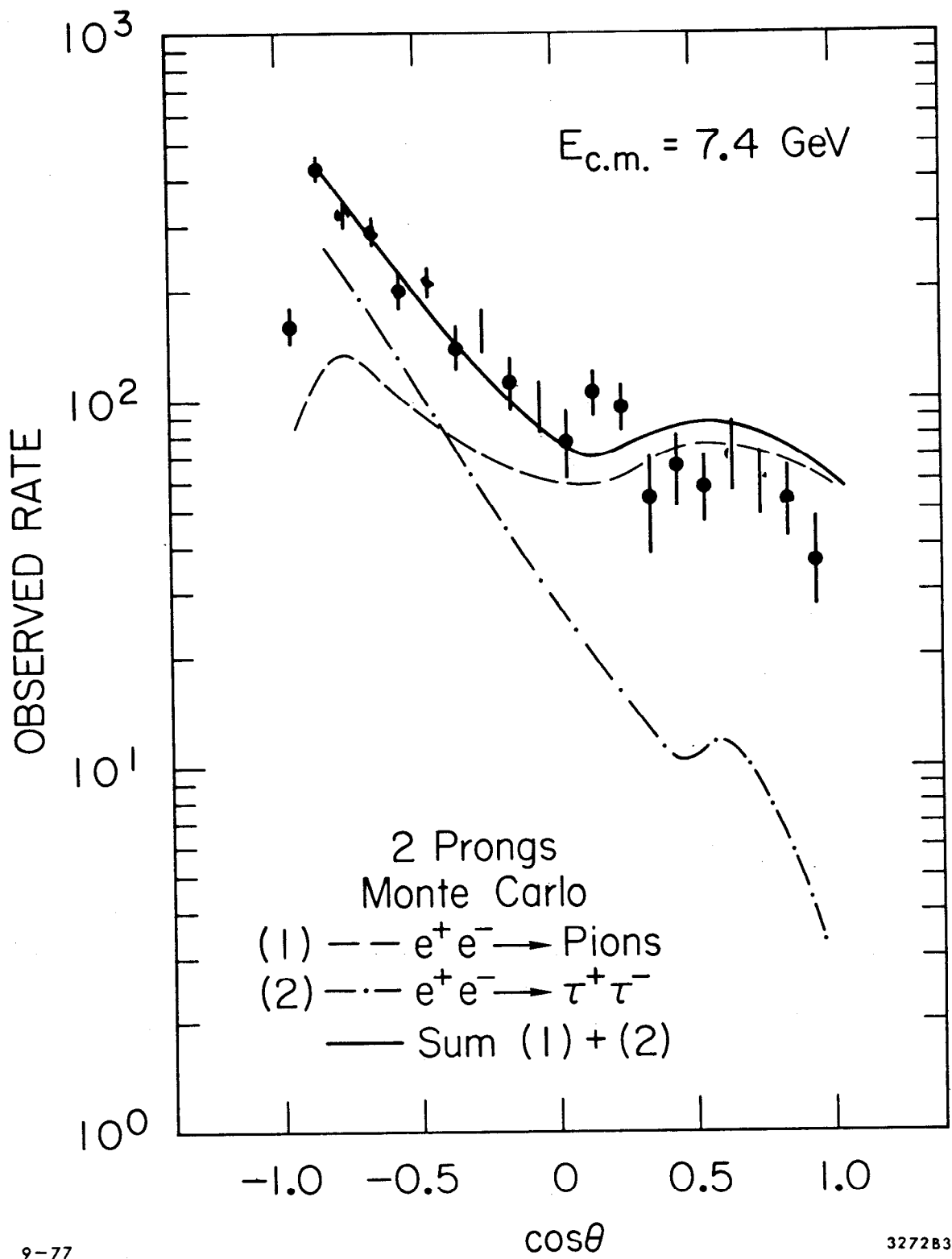
Fig. 5. Comparison of the collinearity angle in two-prong events
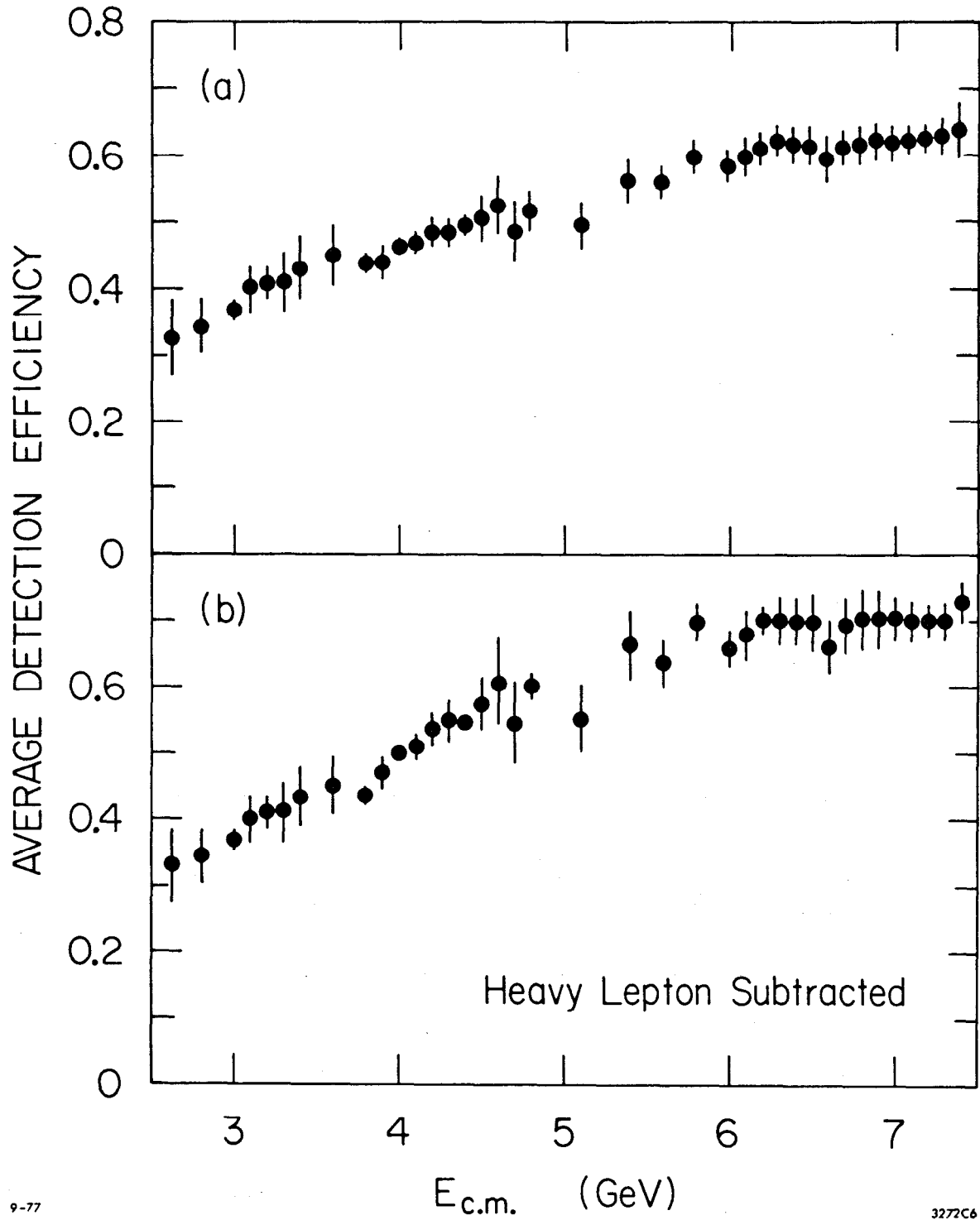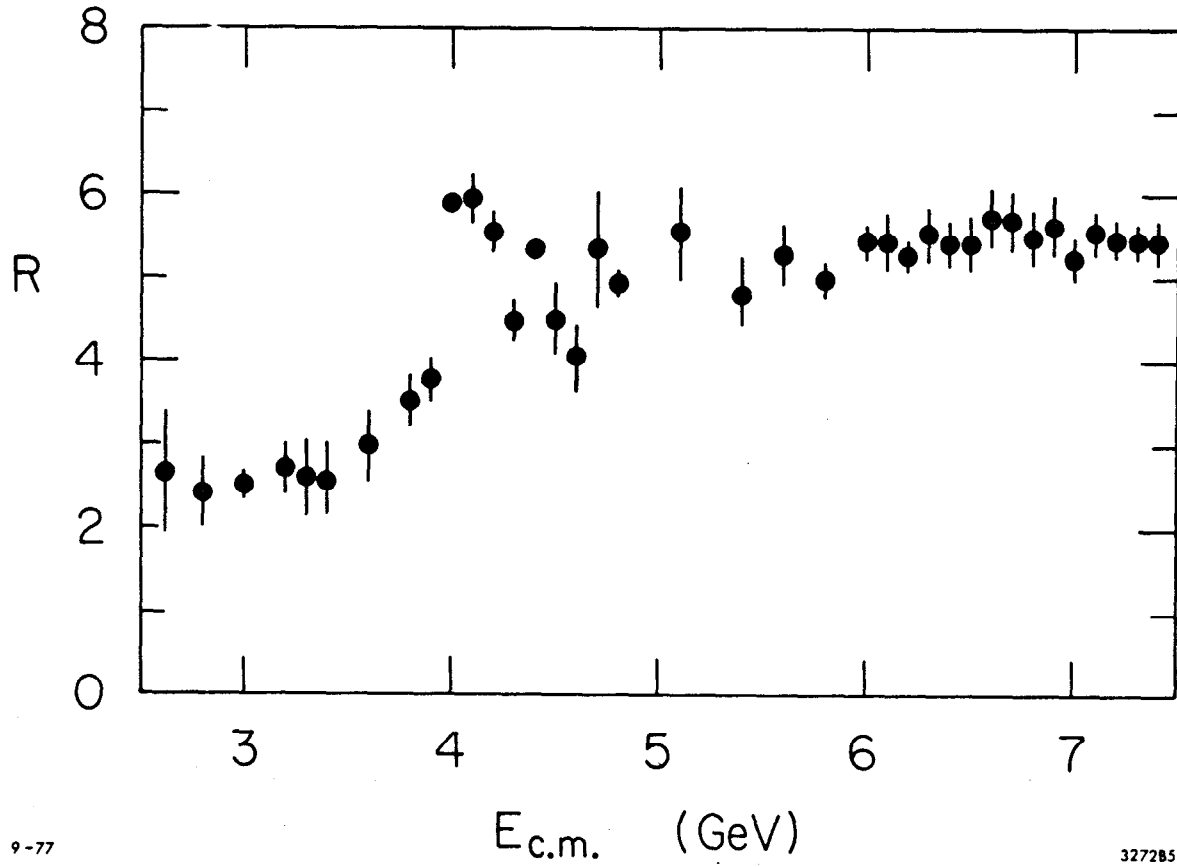at 7.4 GeV in data and model.

Fig. 6. Average detection efficiency for hadronic events as a
function of the c.m. energy : (a) all two and multi-prong
events; (b) heavy lepton events subtracted.

Fig. 7.   The ratio of hadron to μ-pair production cross sections
versus c.m. energy.

of advertisements of a German automobile company, that were published

year after year showing a long list of improvements and changes of the

new model, though to a casual observer the car looks still the same after

more than 20 years. R is approximately constant below 3.5 GeV with a

value around 2.6. Above 6 GeV, R is approximately constant with a value

around 5.5. In between, there is a rather complex structure with peaks

at 4.03 GeV and 4.41 GeV that are related to charm production thresholds.[20,21]

Details are not mapped out here due to somewhat coarser binning in energy.

Radiative corrections have been applied to the data to remove the tails

of the narrow ψ resonances. The errors include statistical and systematic

point-to-point errors. There is an overall uncertainty of ± 10% in the

normalization and there could be an additional variation of up to 10% from

the lowest to the highest energy due to incorrect modeling in the Monte

Carlo.

In Figure 8 the ratio R is presented for the heavy lepton subtracted

data, indicating a plateau of R = 4.5 above 6 GeV, exactly one unit of R

less than before the subtraction. Most of the rise in R near 4 GeV is

observed in the multi-prong data, while the two-prong events show a very

small increase relative to μ-pairs. The data are in general agreement

with the quark-parton model; though quantitatively there may be some prob-

lems since we observe $\Delta R = 1.9$, while we expect only $\Delta R = 4/3$. Likewise

the model predicts R = 2 in the low energy region where we observe R = 2.6.

If we take this measurement at face value and assume that the predictions

of the simple model are uniformly too low by 30%, then we would predict

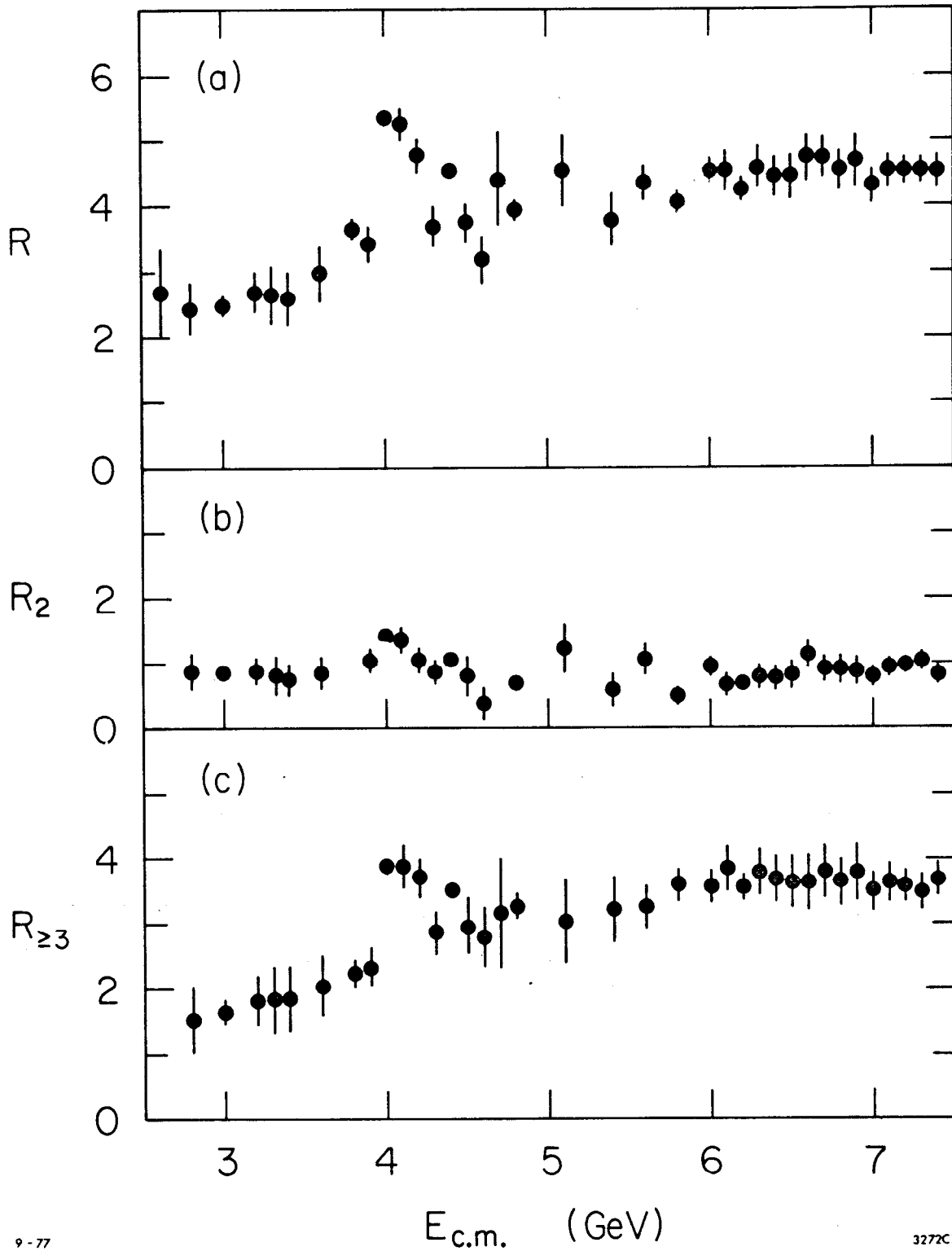a value of R = 4.3 above threshold for charmed particles and find good

Fig. 8 The ratio R for the heavy lepton subtracted data; (a) all
events, (b) two-prongs only, (c) multi-prongs only. The
errors are statistical only.

agreement with the data. In any case, the present uncertainties are too large to draw any decisive conclusion with respect to the quark model.

The data presented here are in good agreement with measurement at DORIS[22,23] below 5 GeV, though our results seem to indicate a somewhat larger value of R. In this comparison, one should take into account that there is very little overlap between the two experiments at the higher energies.

V.   CHARGED MULTIPLICITY

The charged multiplicity distribution of the hadronic final states are obtained from the observed distributions as a by-product of the Monte Carlo analysis that is used to determine $\bar{\varepsilon}$. The energy dependence of the charged multiplicity for all events in the hadronic category (Figure 9) is consistent with the logarithmic rise of the form

$$\langle n \rangle_{ch} = a + b \ln E_{c.m.} ,$$

where a = 2.3 and b = 1.3. A similar parametrization fits multiplicity growth in hadron-hadron interactions.[24] A logarithmic rise of $\langle n \rangle_{ch}$ is a consequence of the limitation in transverse momenta of the produced particles and is expected to set in when their average longitudinal momentum clearly exceeds their average transverse momentum. There is little evidence for a break in the distribution around 4 GeV, though the errors are large and the quality of the fit is fair. If we subtract the expected multiplicity distribution for the heavy leptons events from the observed data, the average produced multiplicity exhibits a step by roughly 0.7 between 4 GeV and 5 GeV. From this we derive an average charged multiplicity of 6.6 for charmed particle production around 7 GeV. This result
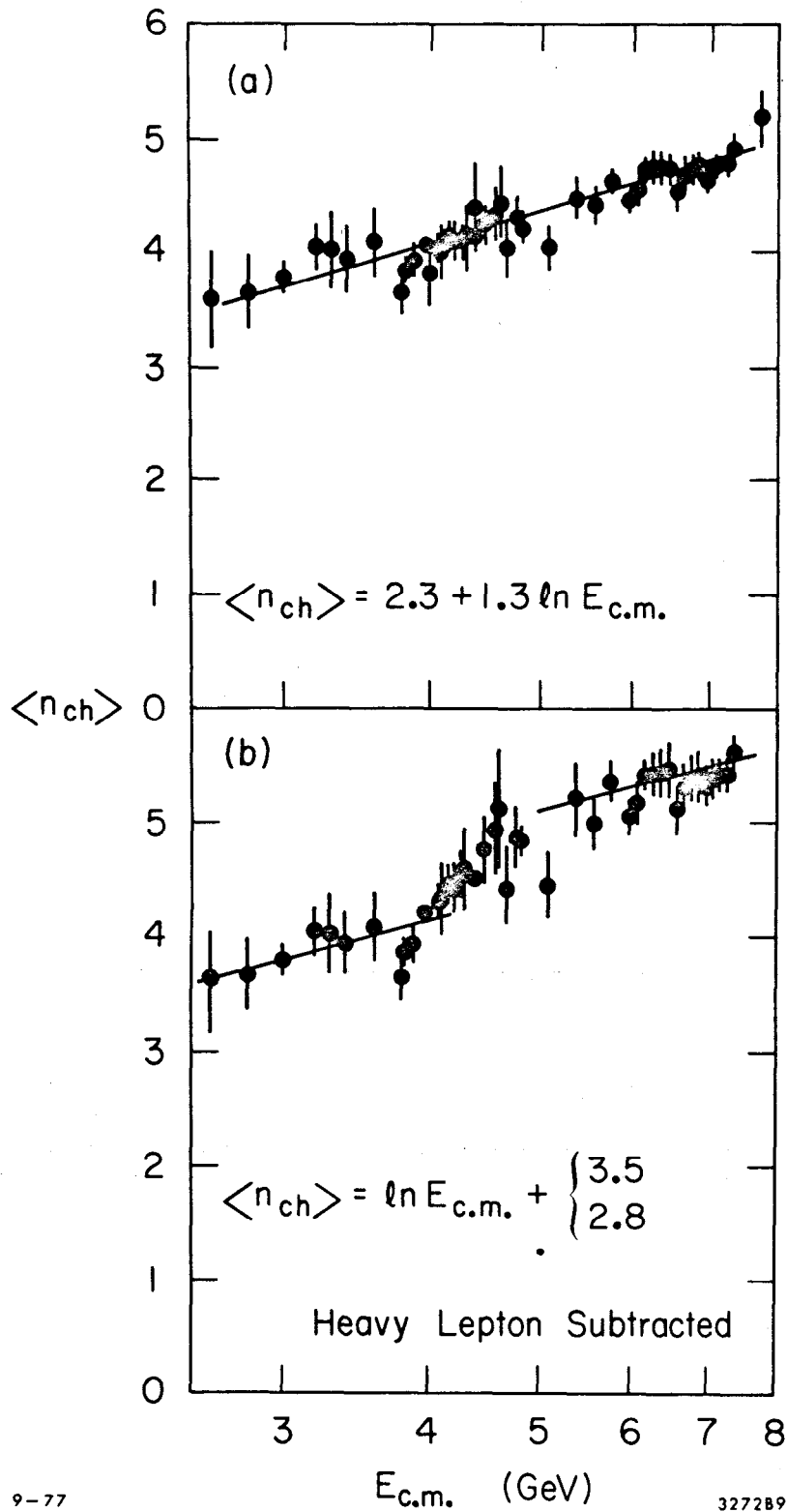
Fig. 9. Average charged multiplicity vs c.m. energy (a) for all
events, (b) for heavy lepton subtracted events.

is supported by a direct measurement of $<n>_{ch}$ for events containing charmed mesons.[25] Thus the smooth rise observed for all events including the heavy lepton can be understood as being the result of a mixture of two new processes, one with low the other with high multiplicity. This has been well confirmed by the study of inclusive lepton spectra.[18]

Examples of charged multiplicity distributions at several c.m. energies are given in Figure 10, with and without the subtraction of the heavy lepton contribution. The unsubtracted data show a surprisingly large fraction of two-prongs, whereas the subtracted distributions resemble the familiar Poisson shape at all energies.

A comparison between multiplicity data from $\bar{p}p$ annihilation[26] and pp interactions[27] and e^+e^- annihilation may provide some insight in the dynamics of hadron production. In Figure 11 the average multiplicity of negative particles is plotted versus energy for the three interactions. The annihilation data show a much higher multiplicity than pp collisions. This is at least partially explained by the fact that there is more energy available in annihilation than in non-annihilation processes. The annihilation data seem to suggest a similar asymptotic rate of increase (i.e. coupling constant) as the hadron-hadron interactions. At low energy the $\bar{p}p$ and e^+e^- data agree well, but the e^+e^- data exhibit a considerably slower rise with energy.

The multiplicity distributions of the annihilation processes are much narrower than those of the pp interactions, indicating that the correlations between the produced particles are different. In order to compare the widths of the multiplicity distributions of various processes,
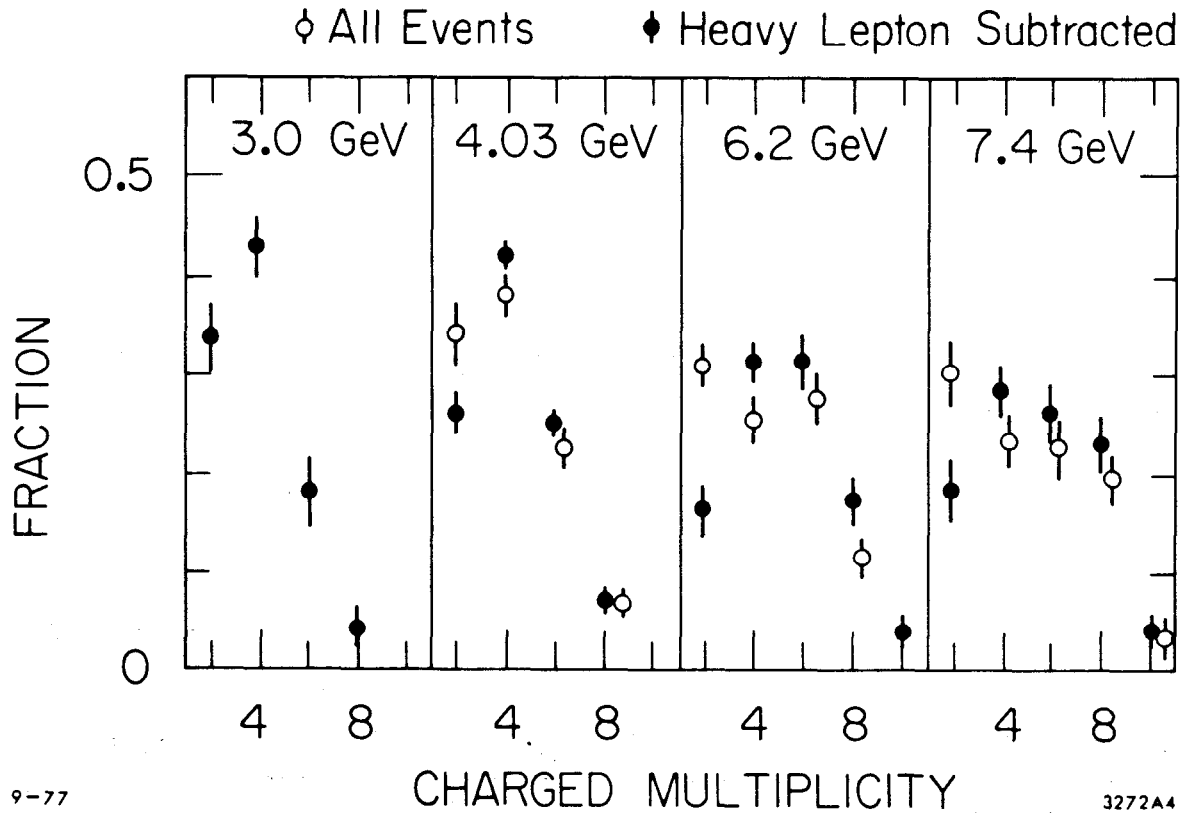
Fig. 10. Charged multiplicity distributions for selected c.m. energies before and after subtraction of the heavy lepton contribution.
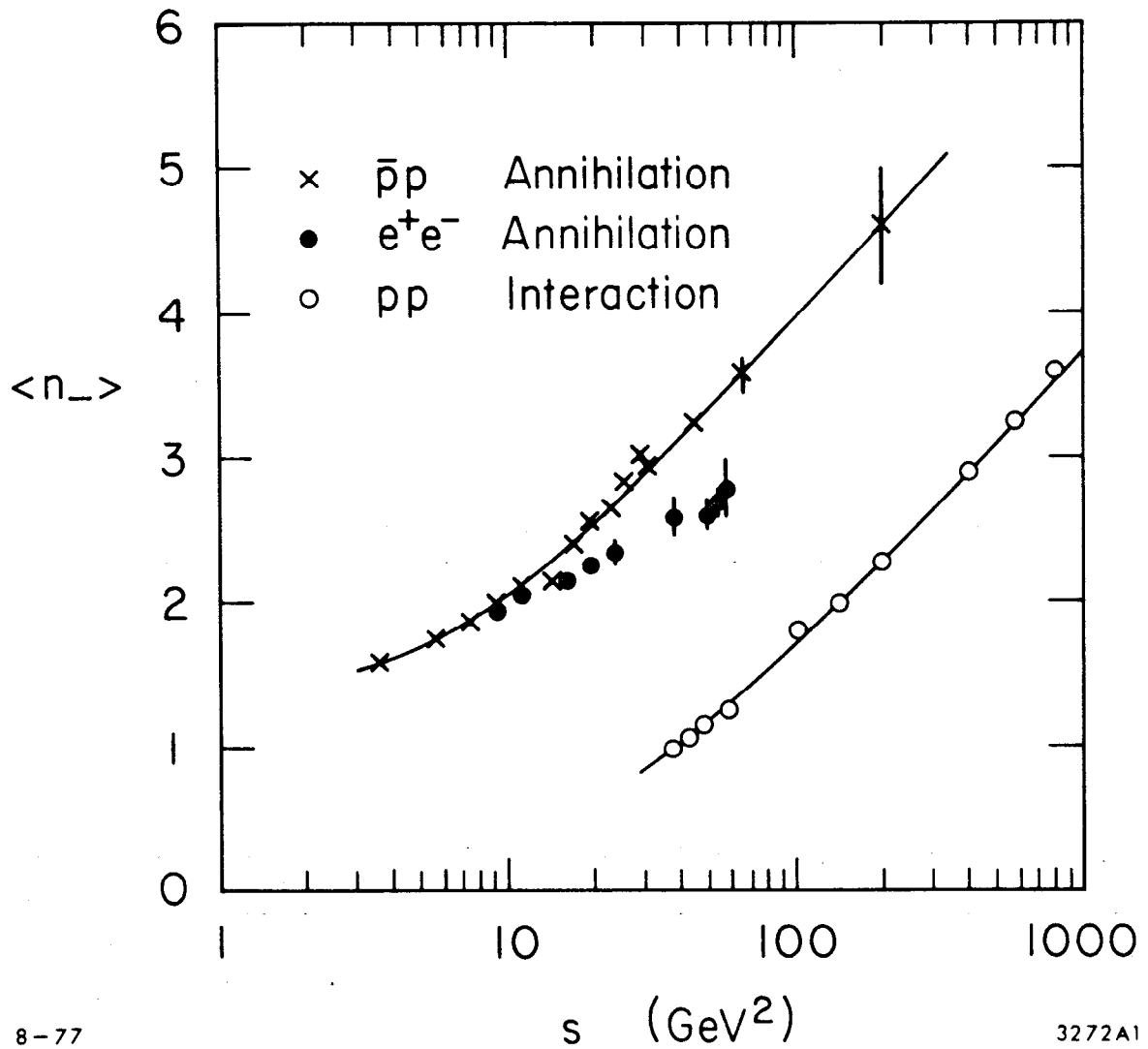
Fig. 11. Average multiplicity of negative particles produced in $\bar{p}p$ [26] and e^+e^- annihilation and pp [27] interactions as a function of c.m. energy. The lines help to guide the eye.

8-77

3272A1

the variable f_2^{--} is plotted versus $<n_->$ in Figure 12, where the correlation integral is defined as

$$f_2^{--} = <n_-(n_--1)> - <n_->^2 = \sigma^2 - <n_->.$$

The $\bar{p}p$ data can be parameterized up to about 60 GeV by a linear function of the form

$$f_2^{--} = a + b <n_->$$

with b = -0.6. It has been shown[28] that this linear fit with negative values of f_2^{--} for low energy annihilation can be understood in terms of a single cluster or fireball formation, i.e., a Poisson-like total multiplicity with no correlation between particles. The large positive values of f_2^{--} for pp scattering are seen as a consequence of multiple cluster or resonance formation and long-range correlations due to inelastic diffraction and non-diffractive production. Each cluster has its own negative value of f_2^{--} but averaging over several clusters gives a positive f_2^{--}. As one reaches sufficiently high energy one might expect to see f_2^{--} for annihilations to deviate from its linear function and turn to positive values. The recent $\bar{p}p$ data at 100 GeV/c are suggestive of an onset of this type of behavior. The e^+e^- annihilation data indicate a similar deviation from the single cluster behavior in an energy range where jet-like correlations have been observed.

VI. INCLUSIVE MOMENTUM SPECTRA

Single charged particle momentum distributions have been studied at SPEAR for large samples of multihadron final states recorded at different
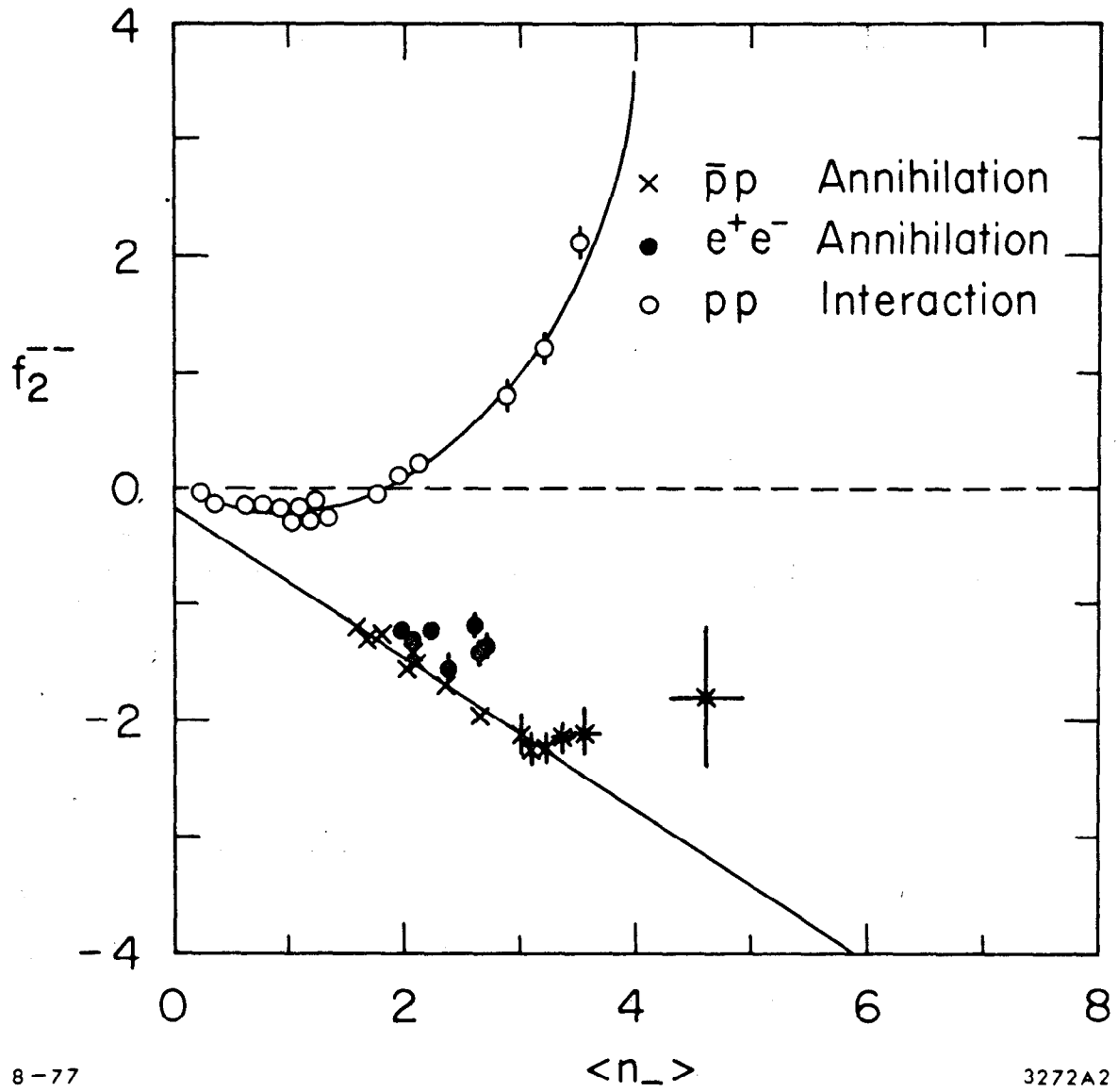
Fig. 12. The correlation integral f_2^{--} vs $<n_->$ for $p\bar{p}$, e^+e^- and pp collisions.

c.m. energies. The data are presented in terms of the scaling variable
x defined as

$$x = 2p/E_{c.m.} .$$

This particular definition has been chosen because in general the momentum
of the particle, not its energy is measured. The results are presented
for the quantity s $d\sigma/dx$ which is expected to scale at high energies.
The integral of this function can be written as

$$\int s \; d\sigma/dx = <n>_{ch} \cdot s \cdot \sigma_{had} .$$

The area under s $d\sigma/dx$ must increase with s, because both the mean
charged multiplicity and s $\cdot \sigma_{had}$ increase.

The efficiency for the detection of a single charged particle has
been evaluated by Monte Carlo, the result is shown in Figure 13 for two
extreme energies. ε varies smoothly as a function of x, with a sharp
decrease below 150 MeV. The uncertainties in ε could be as large as 20%
for the lowest and highest values of x, varying smoothly with x. These
uncertainties are mostly caused by uncertainties in particle tracking and
the model calculations. The data are presented in Figure 14 with purely
statistical errors. The spectra for all energies rise sharply at small
x, peak below x = 0.2, and then fall with increasing x. The area under
the curve grows significantly as expected from the sum rule, but almost
all of the increase is in the low x region. Above x = 0.2, the spectra
are independent of energy for $E_{c.m.}$ greater than 4 GeV. For $x \geq 0.5$ the

SINGLE PARTICLE EFFICIENCY

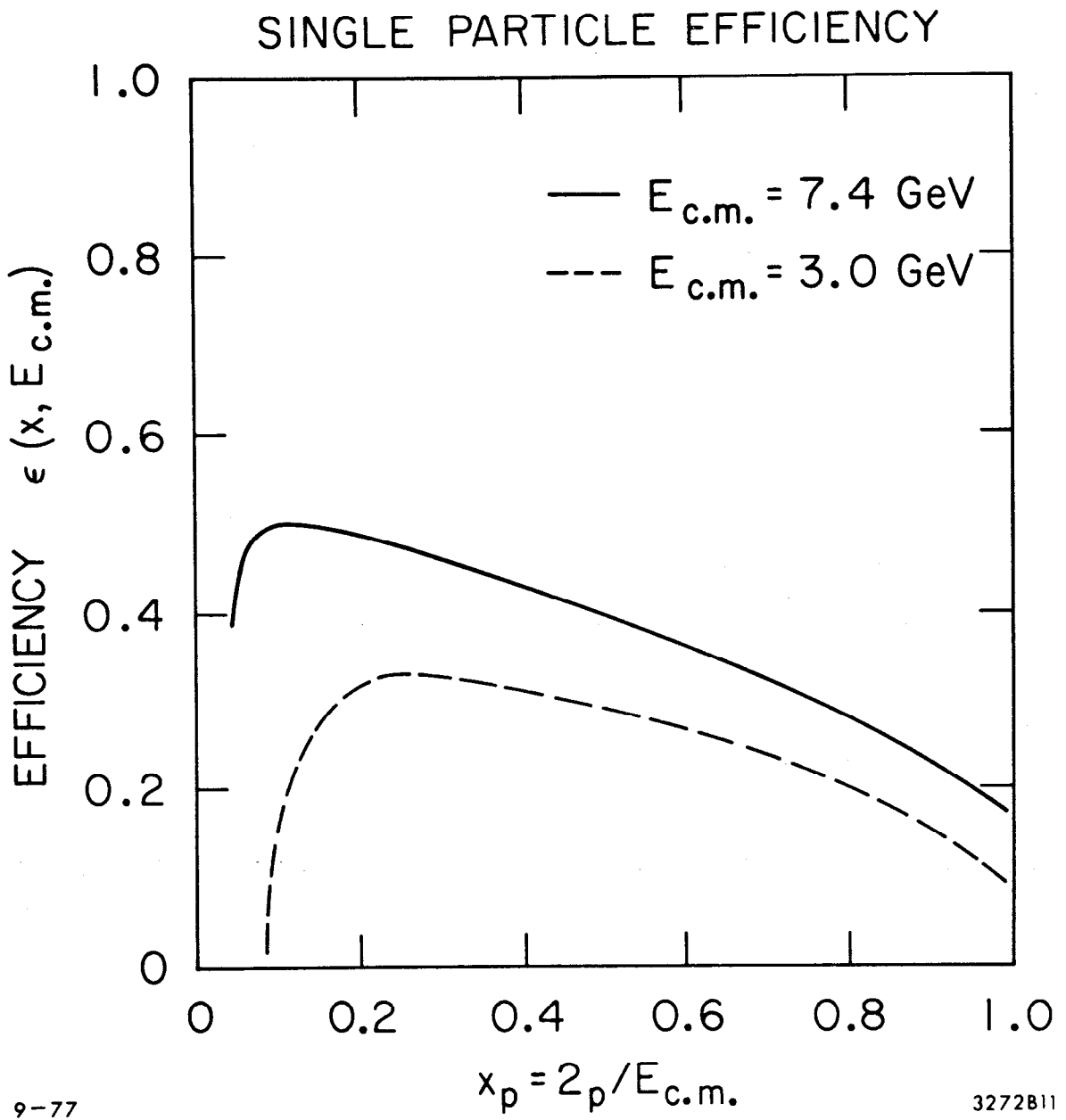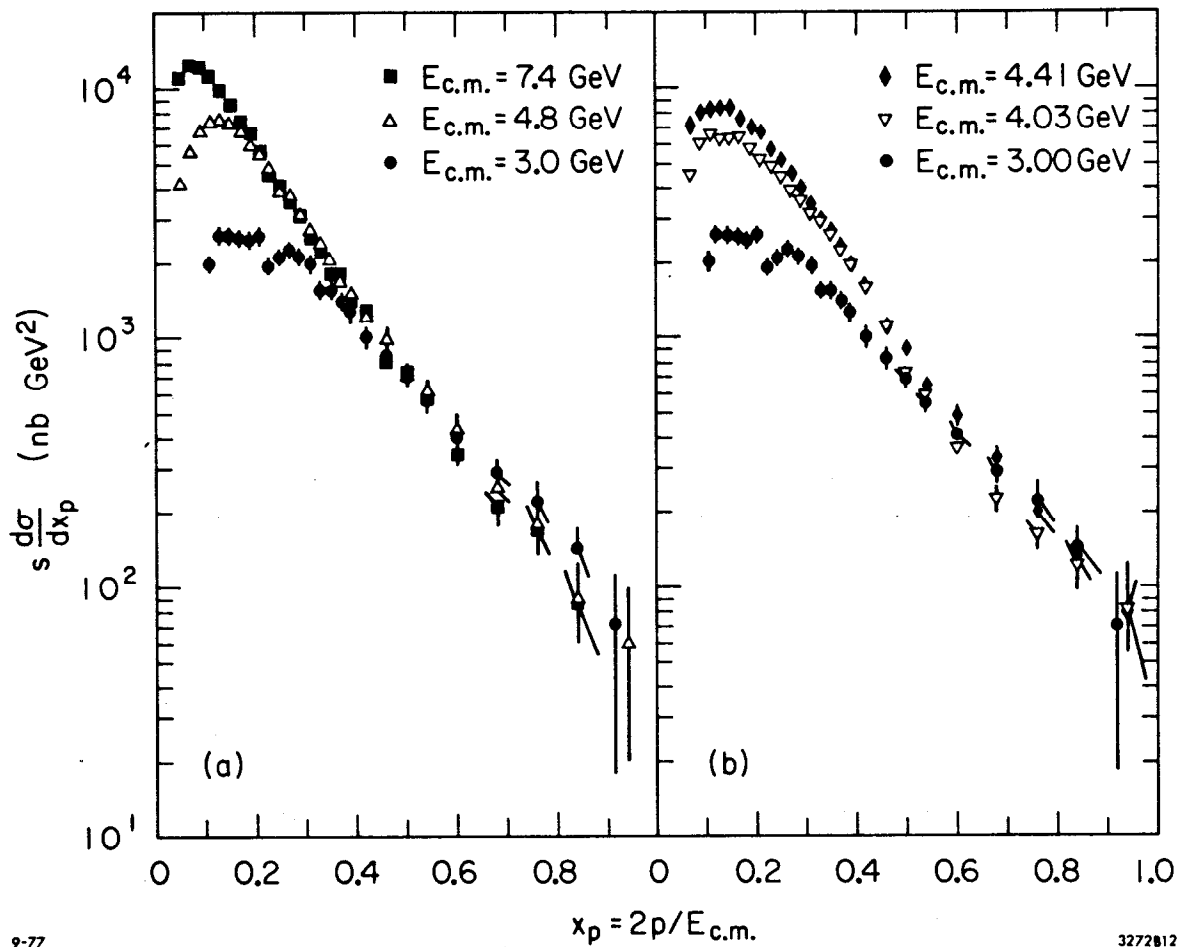Fig. 13. Single particle efficiencey $\varepsilon(x, E_{c.m.})$ for 3.0 GeV and 7.4 GeV c.m. energy.

9-77   3272B11

Fig. 14. Test of scaling in inclusive momentum spectra of charged particles, s dσ/dx for various c.m. energies.

data scale to within 20% over the entire energy range. This is rather remarkable considering that the ratio R changes dramatically around 4 GeV. On the other hand, we know that the pair production of charmed particles near threshold is confined to small values of x. At higher energies the spectra for the decay products of charmed particles seem to be not too dissimilar from all other particles produced. The cross sections presented here are somewhat larger than those of the DASP experiment at DORIS.[29] The same trend was observed in the total cross section data and are most likely related to differences in the overall detection efficiency and normalization.

VII. INCLUSIVE K° AND Λ° PRODUCTION

The SLAC-LBL collaborations have recently reported measurements of the production of neutral K mesons[30] as well as Λ hyperons and protons.[31] These measurements are important in their own right, but are of particular interest in e^+e^- annihilation as a probe for thresholds for the production of pairs of charmed particles. The lowest-mass particles carrying the quantum number charm should decay weakly to states of non-zero strangeness. The thresholds for the pair production of charmed mesons should therefore cause a rise in K meson production, whereas charmed baryons should give an increase in the production of Λ hyperons and protons.

1. Inclusive K° Production

The study is based on large data samples of multiprong events recorded between 3.0 GeV and 7.6 GeV c.m. energy. Neutral kaons are identified by their decay $K_s \to \pi^+\pi^-$. Cuts on the reconstructed decay vertex and the effective mass of the pion pair are applied to suppress background from pions produced directly. For a 20 MeV/c^2 wide interval centered on the

K° mass the signal to background ratio amounts to roughly 5.0. The observed width of 18 MeV/c^2 (FWHM) agrees well with the estimated resolution of the detector. The purity of the K_S sample is obtained at the expense of a rather low detection efficiency. ε is essentially zero below 100 MeV/c, it rises smoothly and reaches a maximum of roughly 25% at 1 GeV/c momentum. A cut at 200 MeV/c is applied to the data, the loss of low momentum K_S has been estimated by extrapolation of the invariant spectrum to zero momentum. The correction amounts to 4% or less.

The results in terms of a comparison of the inclusive kaon production to total hadron production and to muon pair production are given in Fig. 15. The errors indicated include statistical errors added in quadrature to systematic uncertainties. These systematic errors are estimates of the point-to-point fluctuations which arise from the background subtraction and corrections for losses due to cuts. The errors are consistent with the reproducibility of the results under various other selection criteria. Not included is the 15-20% uncertainty in absolute normalization, mainly due to our lack of knowledge about the multiplicity and dynamics of final states containing neutral kaons.

We assume an equal number of K_S and K_L and define $f_K = 2\sigma_{K_S}/\sigma_{had}$ and $R_K = 2\sigma_{K_S}/\sigma_{\mu\mu}$. Above 4 GeV, where most of the data have been recorded, there is roughly one K_S for every four hadronic final states. The ratio R_K is roughly constant at a value of 2.2 for energies above 4 GeV, except at 4.028 GeV and 4.415 GeV where we observe significant deviations from this average. Below 3.8 GeV, R_K is smaller by more than a factor of two, though the statistics are very limited.
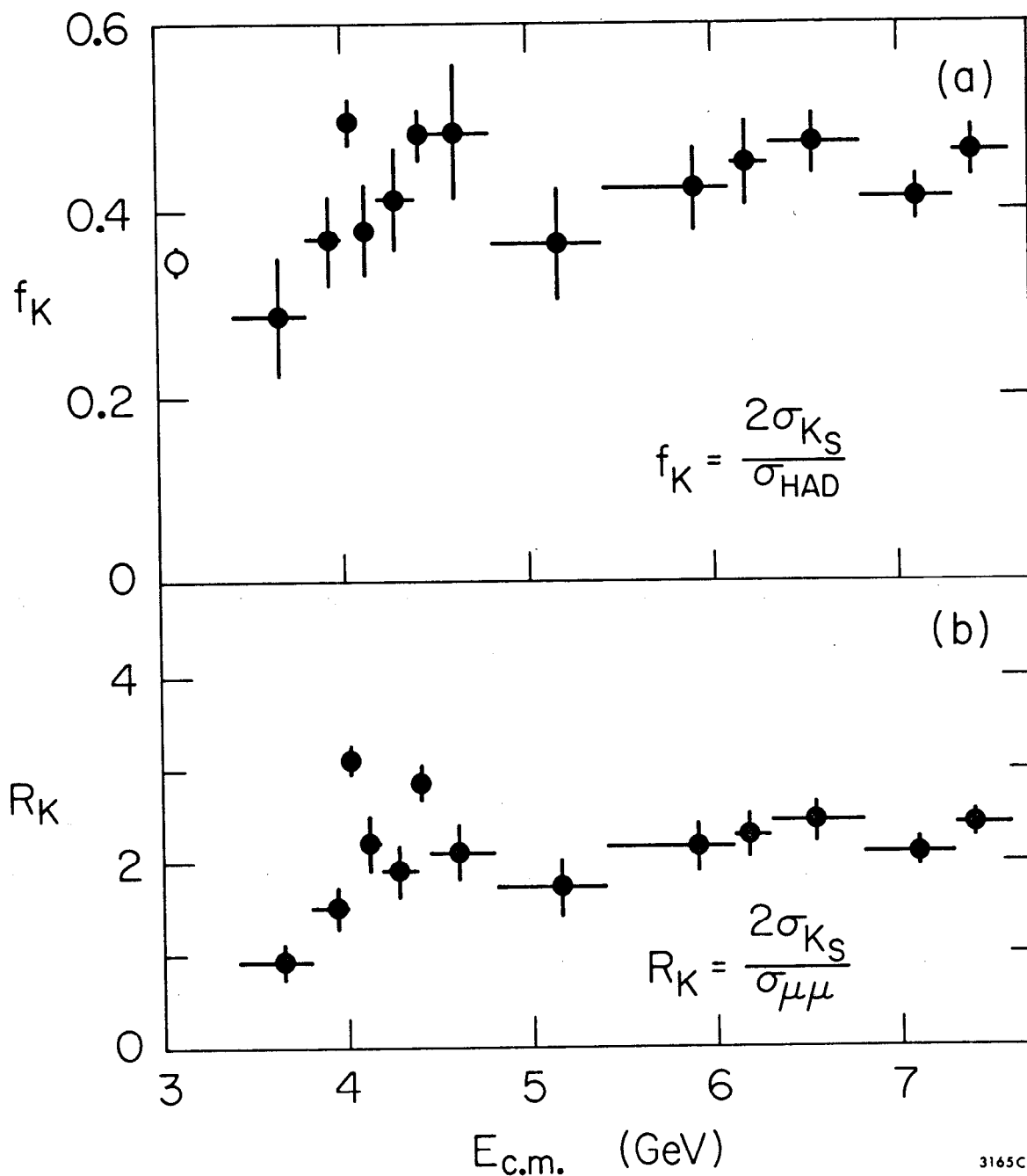
Fig. 15. Inclusive production of neutral kaons as a function of c.m. energy; (a) ratio of kaon to total hadron production, (b) ratio of kaon to μ-pair production. Errors include systematic uncertainties. The data point at 3.1 GeV refers to the $\psi(3095)$ resonance.

A difference between the data recorded at the center of the peaks at 4.028 GeV and 4.415 GeV and the data in the high energy plateau can also be found in the inclusive energy distributions. In Fig. 16 the data are presented in terms of the scaling variable $x_E = 2E_K/E_{c.m.}$, where E_K denotes the kaon energy. Again, the K_S rates have been doubled to obtain the neutral kaon cross sections. Beyond $x = 0.6$ the spectra agree for all c.m. energies. At low x, however, the 4.028 GeV and 4.415 GeV data are strongly enhanced compared to the data sampled below 4 GeV and above 6 GeV. A similar behavior has been found for charged pions and kaons.[15,29,32]

Assuming that the production of charged kaons is equal to neutral kaons, we have used the neutral kaon spectra to correct the spectra of all charged particles for their kaon content and thereby obtain the charged pion spectra. In Figure 17 the inclusive energy spectrum for charged pion is compared to the inclusive K° spectrum in the high energy data. The two spectra are different by roughly a factor five but follow the same slope.

In summary, the inclusive neutral kaon production has roughly the same energy dependence as the total hadronic cross section. The rate R_K rises just below 4 GeV, peaks at 4.028 GeV and 4.415 GeV and reaches a plateau above 5 GeV. The observation of similar enhancements in the number of kaons per hadronic event supports the hypothesis that the rise and the structure in total hadron cross section is due to the threshold for associated production of charmed mesons that decay preferentially to final states of non-zero strangeness. The kaon excess occurs for $x < 0.6$, as expected for a decay product of pair produced charmed mesons near
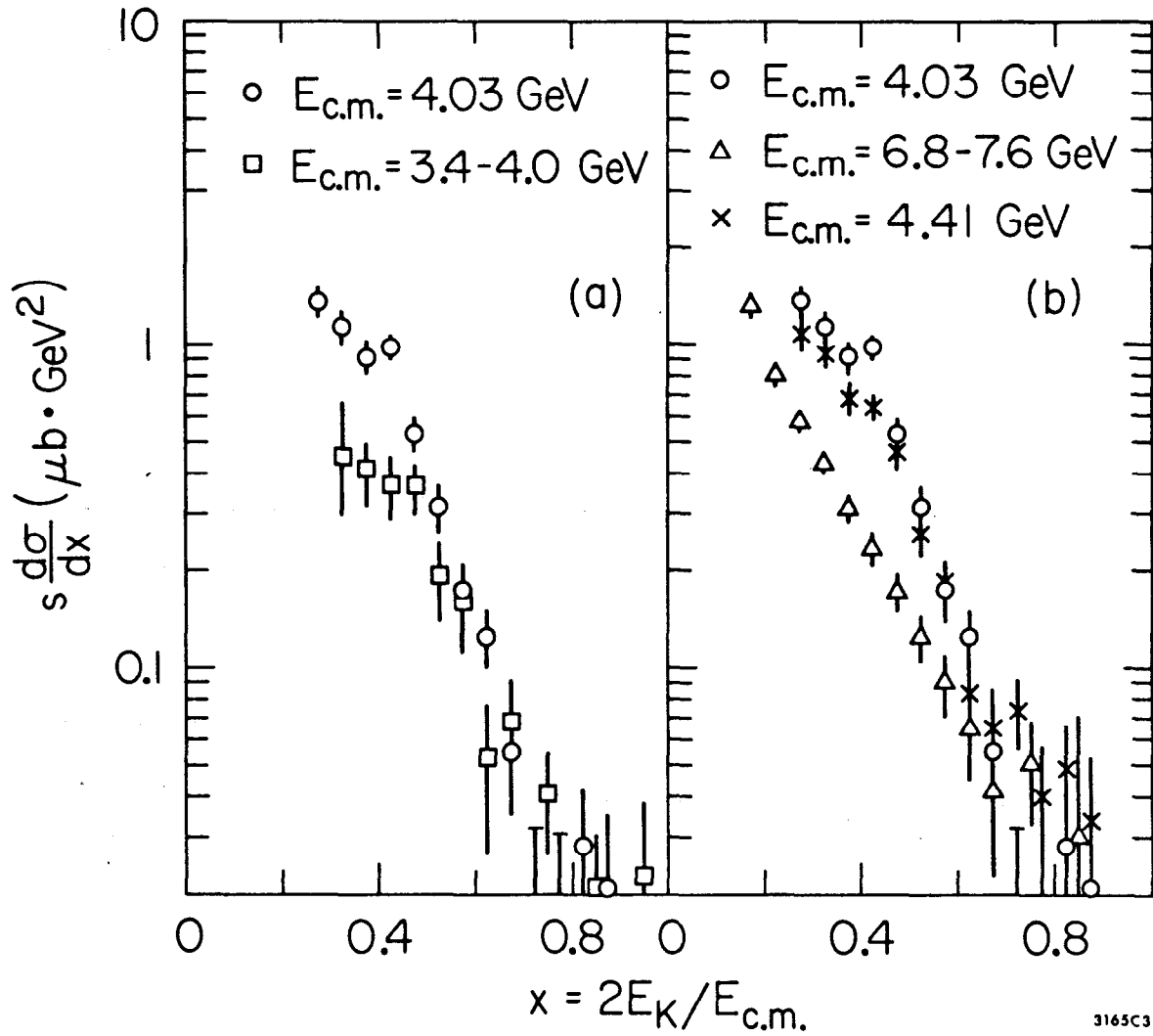
Fig. 16. Inclusive spectra for neutral K mesons as a function of $x = 2E_K/E_{c.m.}$ at various c.m. energies, where E_K denotes the kaon energy and $s = E_{c.m.}^2$. σ refers to twice the K_S cross section. Errors are statistical only.
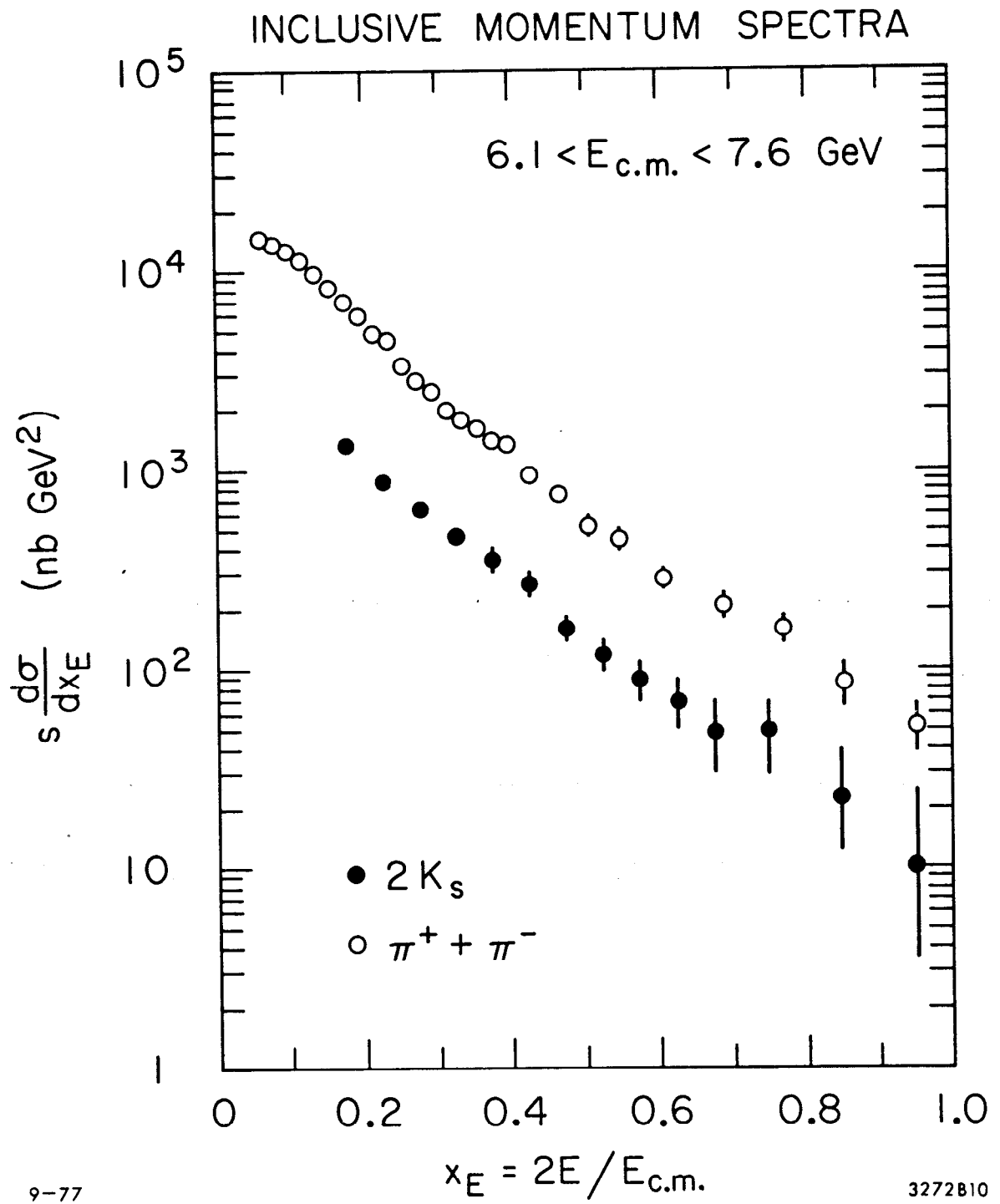
INCLUSIVE MOMENTUM SPECTRA

Fig. 17. Comparison of inclusive momentum spectra of charged pions and neutral kaons above 6.1 GeV c.m. energy.

9—77

3272B10

threshold. This interpretation of the enhanced kaon rates has been confimed by the observation of exclusive decays of the D^o and D^+ mesons.[34,35]

The results presented here are in general agreement with measurements at DESY on inclusive $K^{\pm}$[32] and K_S production,[33] below 5 GeV. Neither DESY group, however, has observed the enhanced kaon yield at the 4.415 GeV structure. This may be due to the fact that their data were not taken at the peak of this resonance, but spread over a much wider range in energy.
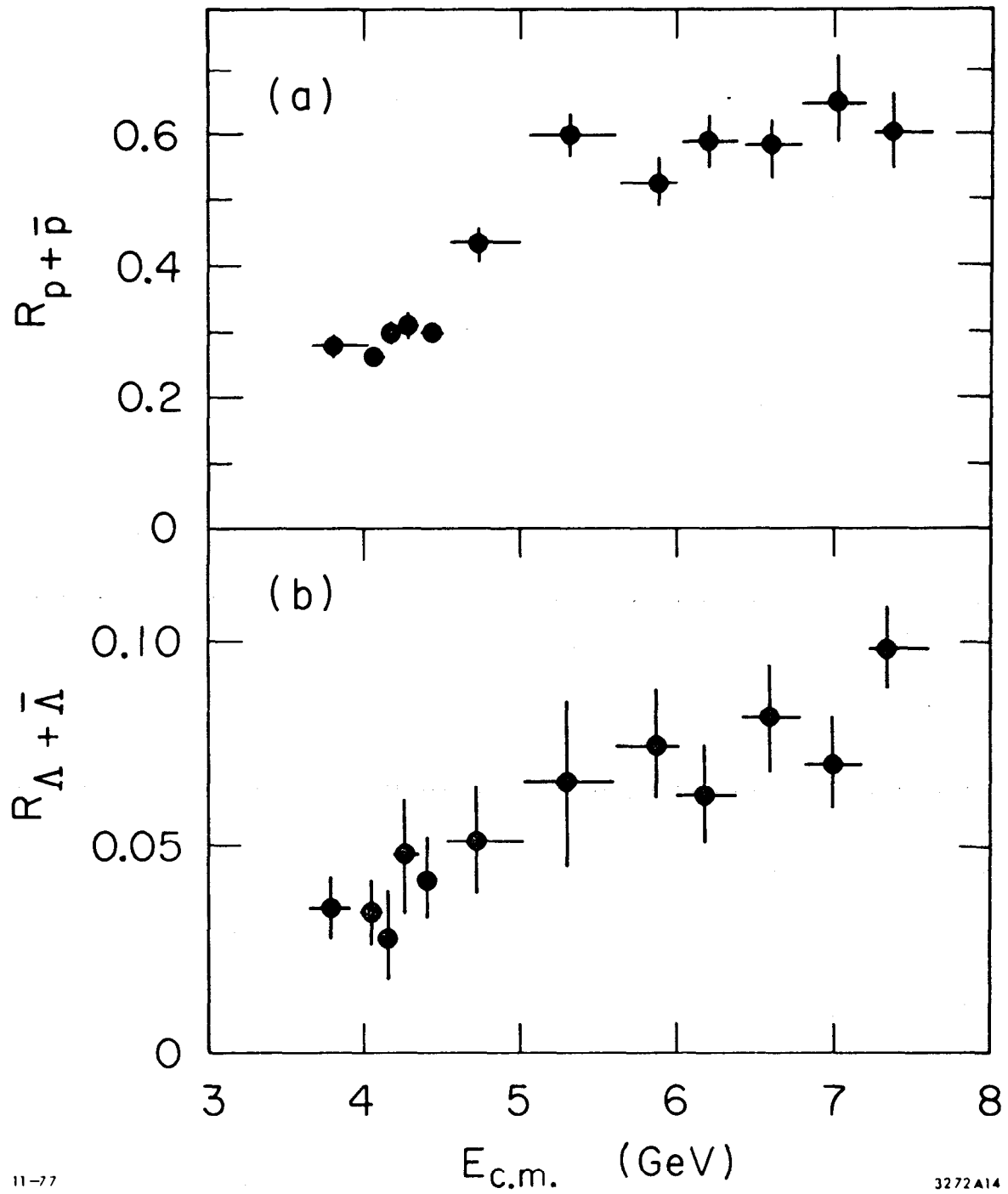
2. Inclusive Baryon Production

Protons and antiprotons are identified with the help of the time-of-flight system. This system consists of 48 scintillation counters arranged in a cylindrical array immediately outside the spark chambers at a radius of 1.5 m from the beam axis. Both ends are viewed by photomultipliers and pulse height and delay times of the signals are measured. As time reference the beam collision time is used which is derived from a pick-up electrode. The system is calibrated with Bhabha scattering events. The rms resolution of the system is 0.35 ns, which allows an unambiguous identification of protons and antiprotons up to 1 GeV/c. For higher momenta the following prodecure has been designed to correct for the limited resolution of the TOF system. Using a Monte Carlo simulation of the detector we compute as a function of momentum a matrix of misidentification probabilities ε_{ij}, where the indices i, j stand for π, k, p. The first index corresponds to the measured mass of a particle, the second gives the true ID of a particle. The diagonal element ε_{ii} of this 3 x 3 matrix give the probability that a particle is correctly identified, while the off-diagonal elements ε_{ij} give the misidentification probabilities.

For low momenta ε_{ij} becomes a unit matrix, whereas for higher momenta the off-diagonal terms become more important. An inversion of these matrices allows us to evaluate the produced spectra of π, k, and p from the observed spectra. This technique deteriorates at momenta above 2 GeV/c where the particle assignment becomes almost random. We therefore estimate the particle yields in this region by extrapolation of the invariant spectra. The above analysis has been carried out for negative particles only, as to avoid background from beam-gas interactions in the proton yields. Λ and $\bar{\Lambda}$ hyperons are identified by their two-body decay. The vertex reconstruction is identical to the K_S decay. In addition, we require that one of the prongs must have a TOF probability of more than 1% for being a p or $\bar{p}$. We have found a sample of almost 1000 Λ and $\bar{\Lambda}$ decays in 350,000 events.

The efficiencies for events containing Λ hyperons or nucleons have been studied with the help of a Monte Carlo program. The lack of knowledge of the production mechanism and the dynamics of final states containing baryons introduces an overall uncertainty of roughly 25%. The detection efficiency for events containing antiprotons ranges from circa 33% at 3.7 GeV to 50% at 7.4 GeV. The Λ efficiency is calculated to be roughly a factor of three smaller.

The results are presented in Figure 18 in terms of $R_p = 2\sigma_{\bar{p}}/\sigma_{\mu\mu}$, the ratio of the inclusive charged nucleon to the μ-pair cross section, and $R_\Lambda = (\sigma_\Lambda + \sigma_{\bar{\Lambda}})/\sigma_{\mu\mu}$, the ratio of the inclusive Λ hyperons production to $\sigma_{\mu\mu}$. R_p shows a rapid rise from roughly 0.3 below 4.4 GeV to 0.6 above 5 GeV c.m. energy. R_Λ appears to have a similar increase, though statistical and systematic errors are much worse. R_Λ is about 10-15% of R_p at all energies. The observation of a rise in R_p around 4.4 GeV, well above

Fig. 18. Inclusive production of baryons as a function of c.m. energy; (a) ratio of charged nucleon to μ-pair production, (b) Λ hyperon to μ-pair production. The errors include statistical and point-to-point systematic uncertainties.

the threshold for charmed mesons near 4 GeV, suggests a baryon threshold near 4.4 GeV. Indeed, candidates for singly charmed, nonstrange baryons have been observed in photoproduction[36] and neutrino interactions.[37]

The most direct evidence for the production of charmed baryons in e^+e^- annihilation would be the observation of peaks in invariant mass distributions of decay products of such baryons. No such peak has been observed, the acceptance of the magnetic detector for the expected decay modes is, however, very low. Therefore, the lack of direct evidence for charmed baryons is still consistent with expected production rates.

If the increase in inclusive baryon cross sections around 4.4 GeV is due to the onset of charmed baryon production the small value of R relative to R_p indicates that their weak decays lead preferentially to nucleons and $\Sigma^{\pm}$ hyperons and not Λ or Σ^0. The easiest explanation for this observation would be a dominant decay of charmed baryons to nucleon, kaon and pions.

VII. SUMMARY

Hadron production by e^+e^- annihilation has developed into an extremely rich and interesting field. The results of the SLAC-LBL experiment at SPEAR can be summarized as follows:

1. Aside from the very narrow resonances ψ (3095) ψ (3684) the variable R, the ratio of hadron to μ-pair production, is approximately constant at a value of 2.6 below 3.5 GeV, and at a value of 4.5 above 6 GeV. These two scaling regions are connected by a region of complicated structure due to charm threshold and resonance formation.

2. Momentum spectra and angular distributions for low multiplicity events clearly deviate from the jet-model predictions and thereby support the existence of a sequential heavy lepton. $\tau^+\tau^-$ production has therefore been subtracted from the hadronic data.

3. The mean charged multiplicity increases logarithmically with energy and after subtraction of the heavy lepton contamination shows a step of 0.7 around 4 GeV.

4. Single particle inclusive spectra exhibit Bjorken scaling for $x > 0.6$ over the energy range from 3.0 GeV to 7.6 GeV.

5. Kaon production follows the rise of the total cross section and shows similar structure near 4 GeV as expected for the charmed meson threshold. Inclusive baryon production suggests a threshold for charmed baryon pair production between 4.5 GeV and 5 GeV.

In summary, general features of hadron production e^+e^- annihilation are well described by the parton model. The regions of constant R, scaling of inclusive spectra and slow multiplicity rise are direct consequences of the parton picture. The size of the step in R between 3.5 GeV and 5.5 GeV is roughly one standard deviation larger than expected. This could either be explained by quark-gluon interactions that are ignored in the simplest model or be the result of measurement errors. We are looking forward to the second generation experiment at SPEAR that is expected to provide us with a more satisfactory answer.

Acknowledgements

The results presented here are based on the work of the SLAC-LBL collaboration (SP-17) that includes the following members:

G. S. Abrams, M. S. Alam, A. M. Boyarski, M. Breidenbach, W. C. Carithers, W. Chinowsky, S. C. Cooper, J. M. Dorfan, G. J. Feldman, D. Fryberger, G. Goldhaber, G. Hanson, J. Jaros, A. D. Johnson, J. A. Kadyk, R. R. Larsen, D. Lüke, H. L. Lynch, R. J. Madaras, H. K. Nguyen, J. M. Paterson, M. L. Perl, I. Peruzzi, M. Piccolo, F. M. Pierre, T. P. Pun, P. Rapidis, B. Richter, R. H. Schindler, R. F. Schwitters, J. Siegrist, W. Tanenbaum, G. H. Trilling and J. E. Wiss.

REFERENCES

1. R. Wilson, Proc. Int. Conf. High Energy Physics; Kiev, USSR (1972).

2. B. Bartoli et al., Phys. Rev. D6, 2374 (1972).

3. C. Bacci et al., Phys. Lett. B44, 533 (1973).

4. F. Ceradini et al., Phys. Lett. B47, 80 (1973).

5. M. Bernardini et al., Phys. Lett. B51, 200 (1974).

6. G. Cosme et al., Phys. Lett. B40, 685 (1972).

7. L. M. Kudadze et al., Phys. Lett. B42, 515 (1972).

8. A. Litke et al., Phys. Rev. Lett. 30, 1189 (1973); G. Tarnopolsky
    et al., Phys. Rev. Lett. 32, 432 (1974).

9. J.-E. Augustin et al., Phys. Rev. Lett. 34, 764 (1974); J. Siegrist
    et al., Phys. Rev. Lett. 36, 700 (1976).

10. J. Burmester et al., Phys. Lett. 66B, 395 (1977).

11. W. de Boer, talk presented at this conference.

12. J.-E. Augustin et al., Phys. Rev. Lett. 33, 1406 (1974).

13. J. J. Aubert et al., Phys. Rev. Lett. 33, 1404 (1974).

14. G. S. Abrams et al., Phys. Rev. Lett. 33, 1433 (1974).

15. R. F. Schwitters, Proc. 1975 Int. Symposium on Lepton-Photon
    Interactions at High Energies, Stanford 1975, p. 5.

16. S. D. Drell, T. M. Yan, Phys. Rev. 187, 2159 (1969) ibid, D1, 1617
    (1970).

17. G. Hanson et al., Phys. Rev. Lett. 35, 1609 (1975).

18. M. L. Perl et al., Phys. Rev. Lett. 35, 1489 (1975).
    M. L. Perl et al., Phys. Lett. 63B, 466 (1976).
    J. Burmester et al., Phys. Lett. 68B, 297 (1976).
    J. Burmester et al., Phys. Lett. 68B, 301 (1976).
    R. Brandelik et al., Phys. Lett. 70B, 125 (1977).
    G. Feldman et al., Phys. Rev. Lett. 38, 177 (1976).
    J. Jaros et al., submitted to Phys. Rev. Lett.
    M. L. Perl, Invited talk at the Lepton-Photon Symposium, Hamburg
    (1977), SLAC-PUB-2022 (1977).

19. Y. S. Tsai, Phys. Rev. D4, 2821 (1971).

20. M. Piccolo et al., Phys. Lett. 70B, 260 (1977).
     G. Goldhaber et al., Phys. Lett. 69B, 503 (1977).

21. J. Siegrist et al., Phys. Rev. Lett. 36, 700 (1976).

22. J. Burmester et al., Phys. Lett. 66B, 395 (1976).

23. W. de Boer, talk presented at this conference.

24. J. Whitmore, Phys. Reports 10C, 273 (1974).

25. G. Feldman, talk presented at this conference; SLAC-PUB 2000 (1977).

26. J. G. Rushbrook et al., Phys. Lett. 59B, 303 (1975).

27. C. Bromberg et al., Phys. Rev. D9, 1863 (1974).
     C. Bromberg et al., Nuclear Phys. B107, 82 (1976).

28. H. Miettinen, Symposium on $\bar{N}N$ Interactions, CERN 74-18 (1974).

29. R. Brandelik et al., Phys. Lett. 67B, 358 (1977).

30. V. Luth et al., Phys. Lett. 70B, 120 (1977).

31. M. Piccolo et al., submitted to Phys. Rev. Lett. (1977); SLAC-PUB-2023.

32. R. Brandelik et al., Phys. Lett. 67B, 363 (1977).

33. J. Burmester et al., Phys. Lett. 67B, 367 (1977).

34. G. Goldhaber et al., Phys. Rev. Lett. 37, 255 (1976).

35. I. Peruzzi et al., Phys. Rev. Lett. 37, 569 (1976).

36. B. Knapp et al., Phys. Rev. Lett. 37, 882 (1976).

37. E. G. Cazzoli et al., Phys. Rev. Lett. 34, 1125 (1975).